

Application of Neutral Networks to Regression and Classification Problems

FYS-STK3155 - Project 2

Alexander Umansky

Norwegian University of Science and Technology, University of Oslo

(Dated: November 10, 2025)

Addressing the universality of Neural Networks, this work explores performance capacity of a customizable Feed Forward architecture, deliberately abstaining from more sophisticated convolutional or recurrent stages. The training algorithm uses Gradient Descent with adaptive learning rate, regularization and batch sampling. We consider performance on regression and classification tasks, including Runge function in one and two dimensions under Gaussian noise, the binary Wisconsin Breast Cancer and multiclass Iris datasets. Beyond architectural design, the impact of optimization parameters and data processing was found to constrain performance, if inadequate, otherwise beneficial to some capacity, set by problem dimensionality or complexity. Neural networks demonstrate definitive advantage over traditional methods when handling higher-dimensional data or large feature sets. The use of deeper and wider networks for high-dimension inputs or subtle patterns increases the risks of overfitting and sensitivity to noise. Regularization proves effective despite its "primitiveness", though as the only safeguard, its effect is bounded by data dimensionality and signal-to-noise ratio. Manual feature processing was needed, as classification performance relies on qualitative measures such as discriminative value and correlations.

I. INTRODUCTION

Artificial Neural Networks (ANNs) are inspired by biological information processing inside the human nervous system. Each neuron cell has a receiver and transmitter which forwards the signal once a certain activation potential is reached. Analogously, input data enters a network of interconnected nodes which can be regarded as the model itself. Transmission between connected nodes is controlled by activation functions and trigger parameters (weights and biases). Neural networks can adapt to any functional input-output mapping¹, with right network architecture and optimized parameters, effectively shaping the geometry of the *responsive* model. This versatility is the reason ANNs are today applied in almost any type of problem, be it regression or classification. They are particularly powerful for identifying subtle and/or highly non-linear patterns in data, and the advantage over traditional methods only grows for higher dimensional data.

This study extends our previous work on performance of Gradient Descent optimization methods for polynomial regression[2]. There, a model of fixed complexity P was optimized to reproduce the non-trivial shape² of the Runge function $R(x) = \frac{1}{1+25x^2}, x \in (-1, 1)$ using a one-

dimensional dataset perturbed by normally distributed noise $N(0, \sigma \leq 1)$. In the present work, we substitute the polynomial model with an arbitrary network architecture, and probe the Runge function in one and two dimensions $R(x, y) = \frac{1}{1+(10x-5)^2+(10y-5)^2}, x, y \in (-1, 1)$. Should performance of ANNs prove compatible against traditional regression methods at "their own game", this would advocate that universality does not come at the cost of effectiveness in concrete cases.

We explore the statement that an adequate tuning of the network architecture will always yield at least satisfactory performance. To this end, we study how ANNs can be used for classification, diversifying with logistical functions and expanding the input and output dimensions. We consider the standard Wisconsin Breast cancer and Iris flower data sets from *Sklearn* library[4][5] as binary and multiclass problems respectively. Using different test cases and feature inputs will firstly, strengthen our claim, and secondly, show the importance of proper preprocessing and feature selection, as they limit the accuracy training can hope to achieve. Performance metrics will be prediction accuracy, confusion matrices, Receiver Operating Characteristic (ROC) curve and Gain curves.

Besides architecture (i.e. activation functions, triggers, depth and width), several optimization attributes will be tested to achieve best performance. The previous study demonstrated the benefit of adaptive learning rate, especially those combining different moments³ like ADAM. For high dependency among features, addition of regularization constrained the parameter coefficients, thus

-
- [1] The universal approximation theorem states that a neural network with a single hidden layer containing a finite number of nodes can approximate any continuous function on a compact subset of \mathbb{R}^n , provided the activation function is non-linear and bounded[1]. The goal of this project is to explore this statement in the context of several types of problems requiring inputs of different dimensions.
 - [2] The Runge function is a case where polynomial regression of increasing complexity fails to converge, exhibiting amplified oscillations near the edges of the interval. Accurately tracing the shape near the edges, without collapsing the central fit, proved to be a major challenge[2][3].

-
- [3] Setting the learning rate a function the gradient, makes GD methods sensible to the topology of parameter space. Here, moment refers to an exponential moving average of past gradients. Different formulations of moments are best suited for distinct topologies[2][6].

stabilizing the solution and deferring the risk of overfitting to higher complexities. When convergence speed becomes an issue, Mini-batch and Stochastic Gradient Descent should be used, but this inevitably degrades the performance. We will prioritize close fit, resistance to noise, and the previously mentioned accuracy statistics.

II. THEORY AND METHOD

A. Setting up and using Neural Networks

In this section we define the general network build and the universal procedure for optimization, common for both regression and classification usage. We start by assuming arbitrary input and therefore leave activation and cost functions ambiguous.

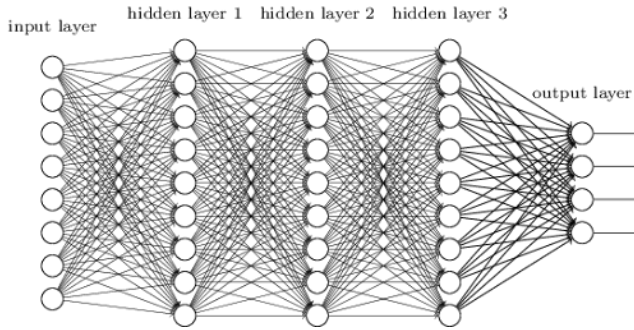


Figure 1: Neural Network with 3 hidden layers. Each node in layer l has n_{l-1} receiving and n_{l+1} transmitting connections, each with specific weight parameter W_{ij} .

A neural network is composed of L layers, such that $l = 0$ is the input layer, while $l = L$ is the final output layer. Layers in between are called "hidden", and the term "depth" refers to the number of hidden layers. Each layer contains n_l nodes which connect as shown in Fig.1. The number of nodes or inter-connections is said to be the "width" of the network. For a general ANN to comprehend both multidimensional and classification data, we define the batched input:

$$X \equiv a^0 \in \mathbb{R}^{n_0 \times m} \quad (1)$$

where m denotes the number of samples in the batch, and n_0 is the number of nodes in the input layer corresponding to data features. Note the difference from a fixed complexity P of a conventional feature matrix $X^{N \times P}$. The complexity of ANNs is not determined by input dimensions, but the entire architecture. Initially arbitrary, through optimization, the functional model assumes the form of the responsive network. On the other end, the number of output nodes corresponds to the dimensionality of the test data, and reflects the outcome for the particular problem, f.ex. number of classes for a classification problem.

Each node in layer l has n^{l-1} connections with the previous layer. When a node receives an impulse vector $a^{l-1} \in \mathbb{R}^{n_{l-1} \times 1}$, it computes the weighted sum z^l and generates a response $a^l = \sigma^l(z^l)$ where σ^l is some arbitrary layer-specific activation function. The response of the j th node in layer l is given by:

$$z_j^l = \sum_{i=1}^{n_{l-1}} W_{ij}^l a_i^{l-1} + b_j^l, \quad a_j^l = \sigma^l(z_j^l) \quad (2)$$

where W, b are trigger parameters defined as:

$$\Theta^l = \{W^l, b^l\}, \quad W^l \in \mathbb{R}^{n_l \times n_{l-1}}, \quad b^l \in \mathbb{R}^{n_l \times 1} \quad (3)$$

W_{ij}^l is the weight of the connection from node i in layer $l - 1$ to node j in layer l , while b_j^l is a bias term that allows neuron response even when its weighted input is zero. This prevents a premature break in the training process. The task of optimization is to adjust these parameters so that the network output a^L best matches some target $Y \in \mathbb{R}^{n_L \times m}$. The process of propagating signals through the network is called Feed-Forward (FF). The model output is evaluated using some cost function $\mathcal{C}(a^L, Y; \Theta)$. We have so far avoided specifying activation functions, but assuming they are non-linear, we use Gradient Descent methods to minimize the cost with respect to the trigger parameters. Because of several nested dependencies, calculating gradients at some layer l requires repeated use of chain rule through all preceding layers:

$$\frac{\partial \mathcal{C}}{\partial (W, b)^l} = \frac{\partial \mathcal{C}}{\partial a^L} \frac{\partial a^L}{\partial \sigma^L} \frac{\partial \sigma^L}{\partial z^L} \frac{\partial z^L}{\partial (W, b)} \cdots \frac{\partial z^l}{\partial (W, b)^l} \quad (4)$$

This procedure is called Back Propagation. Defining $\delta_j^l \equiv \frac{\partial \mathcal{C}}{\partial z_j^l}$, we can regularize the steps. Since,

$$\frac{\partial \mathcal{C}}{\partial z_j^{l-1}} = \sum_k \frac{\partial \mathcal{C}}{\partial z_k^l} \frac{\partial z_k^l}{\partial z_j^{l-1}}, \quad \frac{\partial z_k^l}{\partial z_j^{l-1}} = W_{kj}^l \frac{\partial \sigma^{l-1}}{\partial z_j^{l-1}} \quad (5)$$

where we took the derivative of eq.2, we can express:

$$\delta_j^{(l-1)} = \sum_{k=1}^{n_l} \delta_k^l W_{kj}^l \frac{\partial \sigma^{l-1}}{\partial z_j^{l-1}} \quad (6)$$

Using $\frac{\partial z_j^l}{\partial W_{ij}^l} = a_i^{l-1}$ and $\frac{\partial z_j^l}{\partial b_i^l} = 1$, the GD layer update:

$$\begin{aligned} W_{jk}^l &\leftarrow W_{jk}^l - \eta' \frac{\partial \mathcal{C}}{\partial W_{jk}^l}, & \frac{\partial \mathcal{C}}{\partial W_{jk}^l} &= \delta_j^l a_k^{l-1} \\ b_j^l &\leftarrow b_j^l - \eta' \frac{\partial \mathcal{C}}{\partial b_j^l}, & \frac{\partial \mathcal{C}}{\partial b_j^l} &= \delta_j^l \end{aligned} \quad (7)$$

where η' is some adaptive learning rate computed by one of the algorithms defined in [2][6]. The $a^l, l \in [1, L]$ are known from FF, thus updating trigger parameters goes backwards $L \rightarrow 1$ and $\delta_j^L = \frac{\partial \mathcal{C}}{\partial a_j^L} \frac{\partial \sigma^L}{\partial z_j^L}$ will have unique dependency on the cost and final activation functions.

B. Defining Cost Functions

In the next sections we specify the different activation and cost function that will be used in this study. For regression problem with expected continuous output we keep the Mean Squared Error:

$$\mathcal{C}_{MSE} = \frac{1}{n_L} \sum_{j=1}^{n_L} (a_j^L - Y_j)^2, \quad \frac{\partial \mathcal{C}}{\partial a_j^L} = \frac{2}{n_L} (a_j^L - Y_j) \quad (8)$$

For classification, the output represents a probability vector, hence, the cost function (Cross Entropy) should depend on the negative logarithm of the probability:

$$\mathcal{C}_{CE} = -\frac{1}{n_L} \sum_{j=1}^{n_L} \sum_{c=1}^C Y_{j,c} \log(a_{j,c}^L), \quad (9)$$

where $Y_{j,c}$ and $a_{j,c}^L$ are probability vectors, with c referring to the class label. Binary classification is then a special case where $C = 2$. This formulation implicitly includes the complementary probabilities $(1 - Y) \log(1 - a)$ only if the final activation function is Softmax (see eq.14), where complementarity is ensured by the normalization condition. For this combination, both multiclass and binary backpropagation enjoy a useful simplification[7]:

$$\delta_j^L = \frac{\partial \mathcal{C}_{CE}}{\partial \mathcal{S}_j^L} \frac{\partial \mathcal{S}_j^L}{\partial z_j^L} = \frac{1}{n_L} (a_j^L - Y_j) \quad (10)$$

Regularization can be included in either of the previous cost functions by addition of an extra L1 and L2 norm terms with regularization hyperparameter λ :

$$\mathcal{C}_{MSE/CE}^{\text{regularized}} = \mathcal{C}_{MSE/CE} + \lambda \begin{cases} \|W\|_2^2 & (\text{L2: Ridge}) \\ \|W\|_1 & (\text{L1: Lasso}) \end{cases} \quad (11)$$

Since regularization terms depend solely on W , we need to update only stage 7, note the layer index:

$$\frac{\partial \mathcal{C}^{\text{reg.}}}{\partial W_{jk}^l} = \delta_j^l a_k^{l-1} + \lambda \begin{cases} 2W_{jk}^{l-1} & (\text{L2: Ridge}) \\ \text{sgn}(W_{jk}^{l-1}) & (\text{L1: Lasso}) \end{cases} \quad (12)$$

C. Defining Activation Functions

The universal approximation theorem requires activation functions to be, among other things, continuous and bounded[1]. Bounded range is required to comprehend probability vectors, but it can also serve as an extra level of stability by preventing outputs from blowing up. Had all activation functions been linear, the overall mapping could be expressed as *one* effective linear transformation $Y = W_{\text{eff}}X + b_{\text{eff}}$, thus, the network would not be able

to solve non-linear problems. For non-linear transformations, a classical bounded choice is the Sigmoid function:

$$\sigma(z) = \frac{1}{1 + \exp(-z)}, \quad \frac{\partial \sigma(z)}{\partial z} = \sigma(z)(1 - \sigma(z)) \quad (13)$$

with output range $\in (0, 1)$, it fits naturally in the context of probability. The Sigmoid can be generalized to a case of C classes using the Softmax function:

$$\mathcal{S}(z_i^l) = \frac{\exp(z_i^l)}{\sum_{c=1}^C \exp(z_c^l)}, \quad \frac{\partial \mathcal{S}}{\partial z_j^l} = \mathcal{S}(z_j^l)(\delta_{ij} - \mathcal{S}(z_j^l)) \quad (14)$$

The normalization ensures that $\mathcal{S}(z_i)$ represents a probability vector where $\sum_{i=1}^C \mathcal{S}(z_i) = 1$. Therefore, it is a more universal function that can be reduced to a binary case by setting $C = 2, i = j$ [1]. Both the Sigmoid and the Softmax are "bottle neck" functions that compress the data range. Hence, they are natural for final steps, where Softmax has earlier mentioned benefits.

Both functions can cause vanishing or exploding gradient problems, resulting in extreme training tempo. To mitigate this, common techniques include Gradient Clipping: $\frac{\partial \mathcal{C}}{\partial \Theta} = \min(\frac{\partial \mathcal{C}}{\partial \Theta}, \text{cap val.})$ or placing Batch Normalization before the activation function: $z \leftarrow z - \text{max}\|z\|$.

For simple transmission of signals between hidden layers, one can use linear activation $\sigma(z) = z$, or more commonly, the Rectified Linear Unit: $\text{ReLU}(z) = \max(0, z)$. Since the ReLU gradient is zero for negative z , a node can get "deactivated" by a negative weighted input and never recover[1]. Large initial learning rates might deactivate whole parts of the network for no reason. That is why leaky ReLU is used instead: $\text{LReLU}(z) = \max(\alpha z, z)$, where α is some parameter that allows recovery, as the gradient gradually leaks into the positive domain.

D. Evaluating Classification

Given the final output a^L and labeled target Y , both in $\mathbb{R}^{m \times C}$, the classification accuracy is defined as:

$$\text{Accuracy} = \frac{1}{m} \sum_{i=1}^m \mathbb{I}(\hat{y}_i = y_i), \quad \hat{y}_i = \arg \max_c (a_{ic}^L) \quad (15)$$

where \mathbb{I} is the indicator function that increments when the predicted class matches the target. To analyze performance per class, we use confusion matrices:

$$\text{Binary: } \begin{pmatrix} \text{TP} & \text{FP} \\ \text{FN} & \text{TN} \end{pmatrix} \quad \text{Multiclass: } \begin{pmatrix} n_{11} & n_{12} & \cdots & n_{1C} \\ n_{21} & n_{22} & \cdots & n_{2C} \\ \vdots & \vdots & \ddots & \vdots \\ n_{C1} & n_{C2} & \cdots & n_{CC} \end{pmatrix}$$

Here, rows and columns represent actual and predicted classes respectively. This way, diagonal elements n_{ii} correspond to correct classifications, and off-diagonal $n_{i\neq j}$, misclassifications. A different evaluation scheme, instead of taking the argmax, evaluates based on whether the probability for class i surpasses some confidence threshold t , i.e. $\mathbb{I}(p_i \geq t) = \text{true}$. By sweeping $t \in (0, 1)$ and plotting the True Positive Rate (TPR) against the False Positive Rate (FPR) for each threshold, produces the so called Receiver Operating Characteristic (ROC) curve[1].

$$\begin{aligned} \text{TPR}_c(t) &= \frac{\text{TP}_c(t)}{\text{TP}_c(t) + \text{FN}_c(t)} \\ \text{FPR}_c(t) &= \frac{\text{FP}_c(t)}{\text{FP}_c(t) + \text{TN}_c(t)} \end{aligned} \quad (16)$$

The ROC curve for multiclass classification extends the binary case by iterating over all classes, treating each class in turn as positive while aggregating all other as negative. An ideal classifier maximizes TPR and minimizes FPR, giving a curve that approaches the top-left corner. Diagonal ROC curve describes random guessing. The Area Under the Curve (AUC) quantifies this performance, ranging from 0.5 (random guessing) to 1.0 (perfect classification). Multiclass AUC is calculated by:

$$\text{AUC}_{\text{multiclass}} = \frac{1}{C} \sum_{c=1}^C \int_0^1 \text{TPR}_c(\text{FPR}_c(t)) dt \quad (17)$$

Finally, the cumulative gain curve shows the fraction of positive cases captured when targeting the top α percent of samples ranked by predicted probability[1]. For example: We study N patients for cancer. We select αN "most suspicious" according to some model, and count how many test positive: $P(\alpha)$. This is compared to P cases of cancer cases among N . If the ratio is small, our model is not efficient for determining cancer, not necessarily due to poor features, but because it has low detection rate i.e lacking prioritization of rare positives.

$$\text{Gain}(\alpha) = \frac{1}{C} \sum_{c=1}^C \frac{P_c(\alpha)}{P_c} \quad (18)$$

Here, $P_c(\alpha)$ is the proportion of true positives for class c in the top α fraction of predictions, and P_c is the total number of positives for class c . A sharp gain curve indicates a model that efficiently detects positive cases.

E. Preprocessing

Before training, the batched input must be processed, we standardize each feature column to have zero mean and unit variance. This is done to ensure that each feature initially has equal weighting in the analysis. Furthermore, when regularization is applied, skipped preprocessing might cause unbalanced feature penalization[2][8].

The data is split into training and test subsets using a standard 1:4 ratio. The Model is optimized using the training data, while the test data is used to evaluate how good the model is at generalization by predicting unseen data. Before training, we scale using a 'standard scaler' provided by *Sklearn* library to scale X_{test} and X_{train} . We subtract the mean value from Y_{test} , which will be added later during evaluation as an offset. This prevents scaling from introducing bias into the optimization[8].

The input for classification will go through the same standardization, but first, the features will be selected based on their discriminative power and correlation with other features. In case a variable exhibits high class distribution overlap, we apply logarithmic transformation to enhance separability, before discarding it as a feature. A correlation matrix shows how independent the features are. This is important for a successful classification.

F. Resources

The data used for classification: Wisconsin Breast Cancer data[4], Iris Flower data[5] was retrieved from Sklearn-datasets. We used Keras wrapper for TensorFlow and Sklearn Polynomial regression for comparative analysis with our own NN code. Detailed Imports:

- **Sklearn**[9]: datasets, PolynomialFeatures, StandardScaler, train_test_split, ConfusionMatrixDisplay, roc_curve, auc, RocCurveDisplay, accuracy_score, label_binarize, RocCurveDisplay, roc_curve, auc and LinearDiscriminantAnalysis.
- **NumPy**[10], **Autograd**[11]: grad, norm.
- **Matplotlib**[12], **Seaborn**[13]: mpl_toolkits.
- **TensorFlow (Keras)**[14]: Sequential, Dense, optimizers, regularizers, and EarlyStopping, Hypermodel, RandomSearch from **Keras-tuner**[15].

We also made active use of OpenAI: ChatGPT and DeepSeek to suggest architectures and feature processing techniques.

The code with necessary packages can be accessed here: <https://github.com/4Lexion/Data-Analysis-and-Machine-Learning/tree/main/project2>. The Backpropagation algorithm uses Gradient Descent developed in [2] with modifications made to SDG and Mini-batch methods with *one* batch selection per epoch.

III. RESULTS AND DISCUSSION

A. Regression: Runge 1D

We begin by accessing the advantages of ANNs argued in the theory, and test the different attributes for a simple case of regression for one dimensional Runge function.

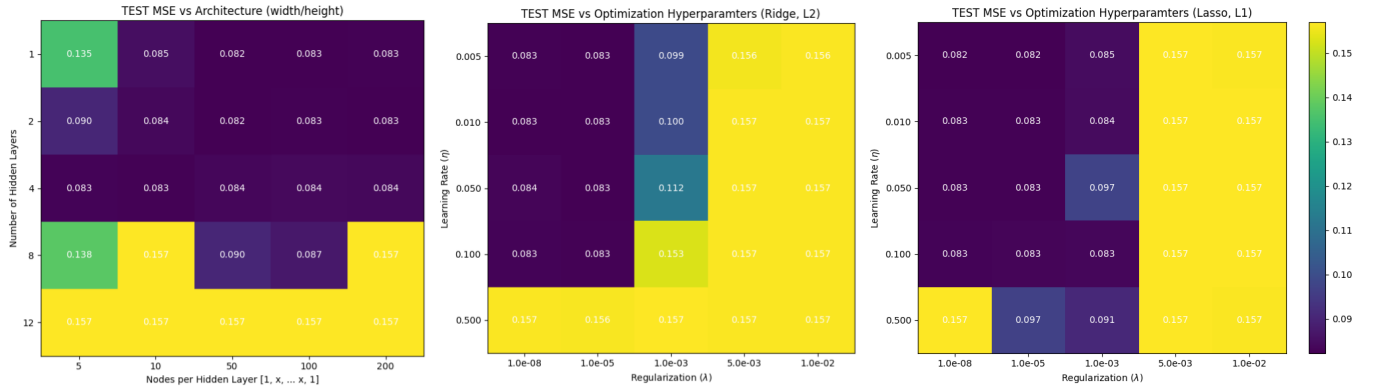


Figure 2: Test-MSE displayed as function of depth and height of the network, learning rate, and L1, L2 regularization. Aside from the axis-parameters, the test uses the scheme defined in Case 1. The dimensions of the network constitute the complexity of the model. Thus, few layers or nodes introduce large bias, making the network to deep results in overfitting. Large λ values should be used to avoid perturbing the optimization, or consider using L1 Lasso. For $\lambda \sim 10^{-5}$ the difference between norms is insignificant. Using ADAM as the adaptive method, gives greater flexibility for learning rate.

Consider Fig.3 where the Mean Squared Test-Error is plotted as function of the sample size N in $x^{1 \times N}$. For the simplified case, Polynomial Regression of $P = 12$, using the analytical expression for Ordinary Least Squares[2] is applicable and serves as a benchmark for satisfactory performance. The blue curve represents a ANN with fixed architecture:

Case 1:

$n_l \in \{1, 50, 100, 1\}$, $\sigma^l \in \{\text{sigmoid, sigmoid, linear}\}$,
ADAM($\eta = 0.05$), $\lambda = 0$, Batch mode

while the green runs the standard library TensorFlow with 5 random selections of (n_l, σ^l, η) and saves the best performing for each new dimension. The analytic solution stagnates, and is increasingly outperformed once the dimensionality is larger than 100. For smaller samples, it is very likely that randomly selected configurations overfit. The fixed architecture was selected to give a stable performance, but it is apparent that at larger N re-optimization yields more favorable performance. This indicates that the architecture that worked for some input dimension is not guaranteed success for others. It is reasonable to anticipate a stronger effects for $x^{n_1 \times M}$.

Unlike polynomial degree, selecting network attributes is less intuitive. The choice of sigmoids for activation functions, enables the ANN to trace the slope of the Runge function more accurately than high-degree polynomials, avoiding buildup of oscillations near the edges. The earlier mentioned bottleneck effect, acts as a high-pass filter in the presence of noise. For the final layer we make use of a linear activation, since the sigmoids already provide the necessary non-linearity.

Fig.2 shows the test-MSE as two dimensional function of learning rate, regularization, depth and width: $MSE(\eta, \lambda)$ and $MSE(L, \{n_l\})$, where for simplicity we consider one n for every hidden layer. When evaluat-

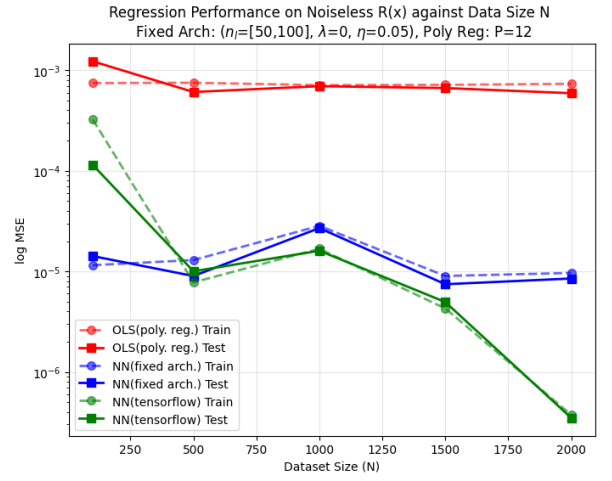


Figure 3: Comparing Test-MSE as function of data size N . The red curve shows the stagnating performance of polynomial regression using analytical OLS against ANNs that improve as dimensionality grows. The blue curve corresponds to a fixed architecture (Case 1) yielding stable performance, while the green re-optimizes network depth and optimization parameters for each new input.

ing the hyperparameters, we use the previously specified architecture of Case 1 with $N = 1000$. Judging by the left plot, best performance is achieved using between 2 and 4 hidden layers with number of nodes between 50, 100, while plot edges generally indicate higher loss. Considering the network as a geometrical shape, the model complexity is the area i.e. depth \times width. Small area represents oversimplification and inherently larger bias, while using too deep or wide network can result in overfitting. We return to this idea in later sections.

The middle and right plot shows effect of regularization used as part of L_2 and L_1 norms. Very large λ values shift the focus of optimization as described in [2]. Since

Lasso used λ^1 , it offers a larger interval of safe values, rather than Ridge, but for $\lambda \sim 10^{-5}$ the effect on MSE is insignificant. The learning rate is crucial for Backpropagation to work effectively. The plots are generated using ADAM which uses a highly robust adaptive scheme and therefore exhibits greater tolerance to initialization. For other adaptive methods, or when using mini-batching, learning rate is generally less flexible.

Without changing the architecture, the comparison of different GD methods for backpropagation is shown in Fig.4 (top). As predicted, ADAM gives the most reliable fit, but RMSProp was shown to be competitive when a stronger noise component ($\sigma = 0.5 - 0.8$) was used. RMSProp lacks the same nuanced scheme as ADAM, which for stochastic data is beneficial. With a smaller learning rate, ADAM in Stochastic mode is also applicable, though it fails to fit the central section and is insufficient for worse signal-to-noise ratio.

The bottom plot, shows what happens if we shift position of the sigmoid activation. We specially used a sample with stronger noise component ($\sigma = 0.8$) to test our theory of it acting as a high pass filter. Indeed, it turns out using it in the first layer has great impact, whereas, adding consecutive in series gives less improvement. This is a very characteristic pattern of filters. The nonlinearity and curvature of the sigmoid makes it a more effective fragment for regression, rather than f.ex. Leaky ReLu, which is also bounded and has properties of a high pass filter. These results will be carried over to higher dimension where we study overfitting and regularization while fixing the usage of sigmoid activation and ADAM with $\eta \in [0.05, 0.01]$.

B. Regression: Runge 2D

The two-dimensional variant of the Runge function is shown in Fig.6. Its profile exhibits two prominent peaks, which we refer to as *signal*, superimposed on a flat *background* broken by stochastic fluctuations. The test data will have two noise configurations $\sigma \in \{0.1, 0.3\}$, to probe the model's susceptibility to overfitting. Ideal model performance is characterized by properly resolved signal peaks, while modeling the noise as flat background.

From the top plot it is clear that a network with two hidden layers is not sufficient to resolve the signal peaks. Hence, we opted for a third hidden layer with sigmoid activation, designing the node layout resembling a "funnel", with fewer nodes for deeper layers. As expected, the larger network area provides the additional model complexity required to resolve the signal, see Fig.6 (mid), albeit with higher sensitivity to the background peaks. Comparing the MSE performance for data with $\sigma = 0.3$, the deeper network exhibits a lower training loss, but an even higher test loss than when using fewer layers. This confirms that the model learns the fluctuations, resulting in a large prediction variance.

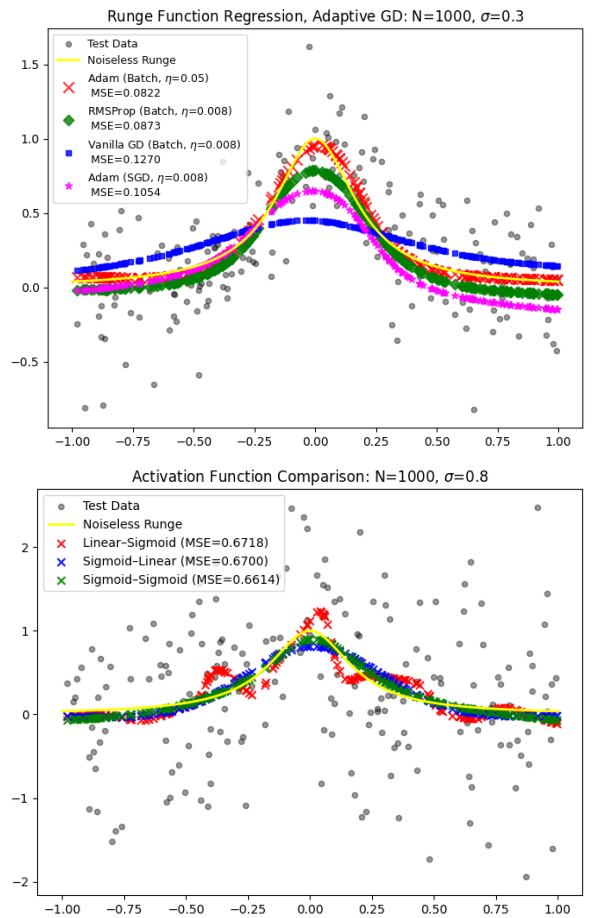


Figure 4: **Top:** Comparing ADAM (batch and stochastic mode) with RMSProp and GD without adaptive learning rate. With the particular learning rates shown in the legend a very good fit is achieved with ADAM and satisfactory performance from RMSProp and Stochastic GD. **Bot:** Using the same architecture as earlier, but changing the placing of the sigmoid activation for a sample with stronger noise component. Using sigmoid in the first hidden layer proves crucial for to achieve good shape tracing. Using it in both further improves but much less. This is very reminiscent of behaviour one would expect from a high pass filter in series.

We explore regularization as an accessible means to alleviate overfitting. Fig.6 (bot) compares the effects of applying Ridge and Lasso methods. Recalling the value constraint in Fig.2, we set $\lambda \sim 10^{-4}$ and examined higher values with $L1$ and $L2$ norms. In both cases, stronger regularization was seen to smoothen the background but degrading the signal fit. However, owing to the prefactors in eq.12, and the more flexible $\text{sgn}(W)$ dependency, Lasso regularization achieves a more favorable tradeoff. A closer look at the bottom-right fit, shows that $L1$ prediction underestimates one of the signal peaks, yet it effectively suppresses several of the most severe background fluctuations. Note, the tradeoff depends on specific dataset distribution, and in general a prioritization of signal efficiency or stable background is unavoidable.

The observed improvement in test loss confirms that regularization is an effective measure. Nevertheless, this benefit diminishes as the noise gets stronger. Regularization should be regarded as a "primitive" solution, easily implementable in any application, but with limited capability. Judging from the trends in regression performance from previous section, optimization for increasingly complex and higher-dimensional problems require larger and deeper networks. The diminishing effectiveness of regularization is insufficient to compensate for the growing network complexity. Application-oriented neural networks include more sophisticated measures in their convolutional or recurrent stages during training, which are not considered during this study[16]. A different approach concerns data representation. If like in this case, distinction between signal and background carries a topological or geometric character, redefining the coordinate system or data representation can serve as an effective means of embedding class separation directly into the data prior to training. An example from quantum information theory, where spherical representation were used for quantum state projection [17].

C. Multiclass Classification: Iris Data

The second type of problem considered in this study is classification. As mentioned in the theory of ANNs, the input layer corresponds to the number of features, while the output layer matches the target classes. The Iris dataset contains $M = 150$ entries, *evenly* classified into $n_L = 3$ flower species: *Setosa*, *Versicolor* and *Virginica*, based on width and length of the flower petal and sepal i.e. $n_0 = 4$ features in total.

Prior to training, we preprocess the features for the reasons specified in section II E. Applying the logarithmic transformation *before* scaling was an attempt to reshape and further separate the distributions without loss of information. However, since all dimensions are recorded in the same unit (cm.), with small base magnitudes, neither logarithmic nor power transformations improved separability beyond what was already visually evident. Alternatively, we applied the *Linear Discriminant Analysis* from *Sklearn*, which projects initial features onto a more discriminative basis built on certain feature combinations. Yet, with only 4 strongly correlated features, this measure did not prove effective.

Fig.7 (top) shows that *Setosa* is distinctly separated from the other two classes, while *Versicolor* and *Virginica* have a great overlap based on sepal measures, with less critical overlap in petal features. The correlation matrix, Fig.7 (bot), indicates strong feature correlations. The petal dimensions are in particular, dependent on other features. Although, redundancy is evident, without substitutes, removing features would risk loosing discriminative information in an already sparse dataset.

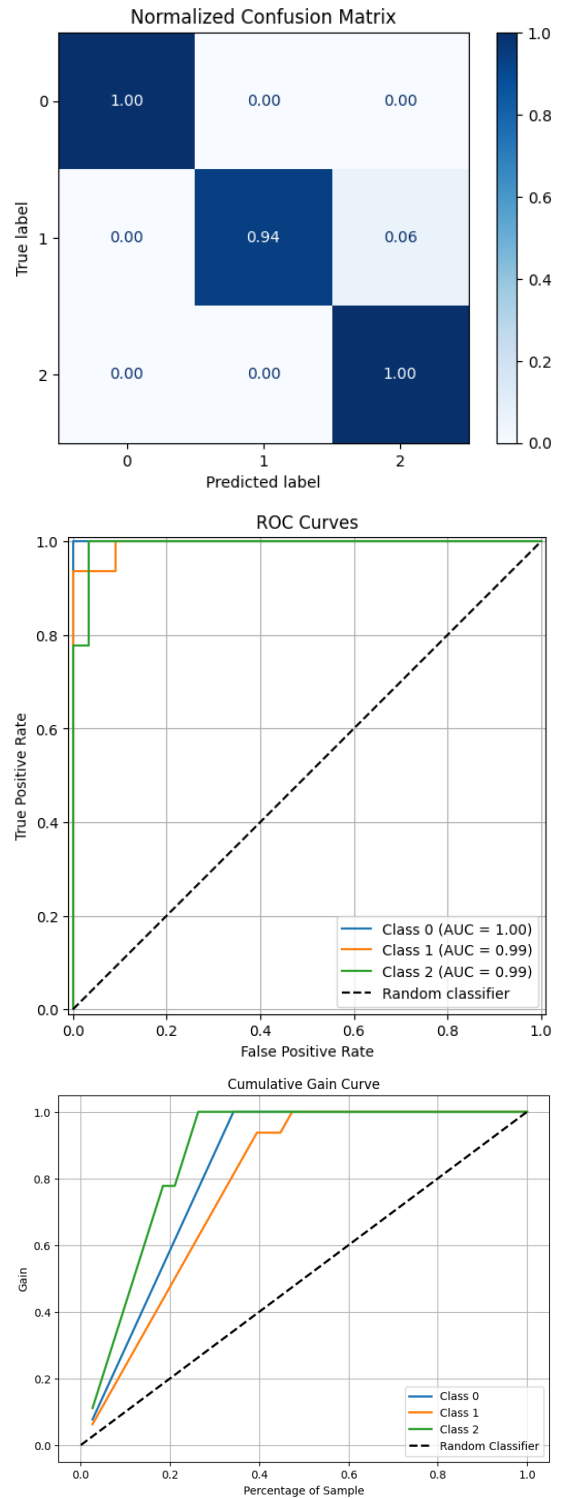
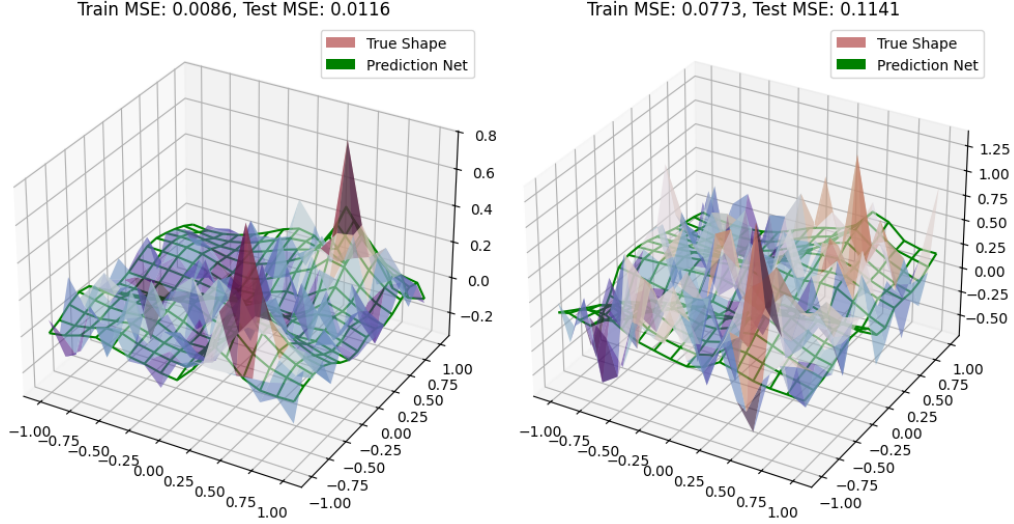
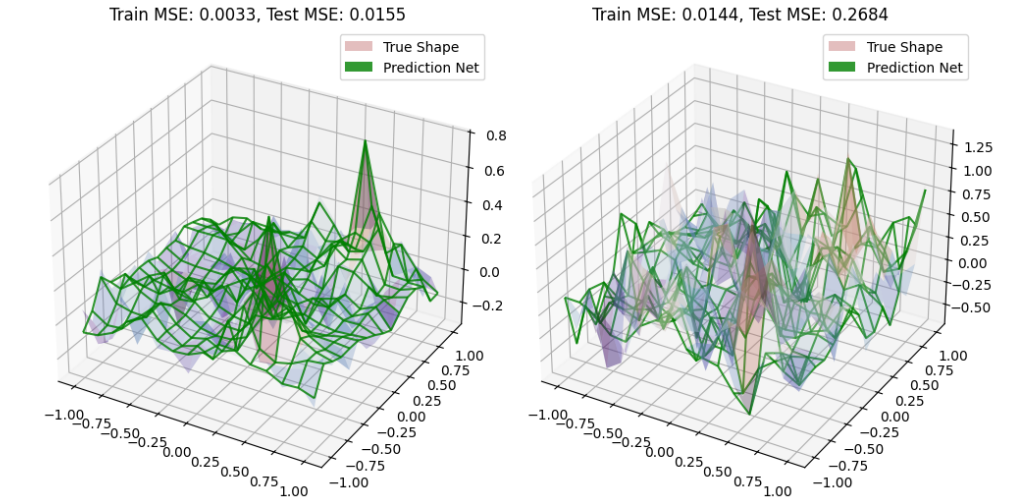


Figure 5: Performance of ANN multi-classification on the Iris dataset. Due to small number of features and entries $n_0 = 4, M = 150$, prediction accuracy of 97% can be achieved using a single hidden layer with few nodes, see Case 2 for detailed configurations. **Top:** Confusion matrix shows dominant diagonal elements corresponding to correct classifications, with some of class 1 misclassified as 2, the two classes with most overlapping distributions. **Mid:** ROC curve with $AUC \approx 1$. Class 0 with most distinct separation yields the best classification confidence. The other classes also exhibit solid classification performance. **Bot:** The Gain Curves show that > 0.9 of all true positives are recovered with $0.2 - 0.3$ of the data. Class 2 has fastest gain, likely due its entries having less variance and fewer outliers.

$R(x, y, \sigma = 0.1/0.3)$, Arch:[2, 50^{sgm.}, 100^{sgm.}, 2], $\lambda=0$, $\eta(\text{ADAM})=0.01$



$R(x, y, \sigma = 0.1/0.3)$, Arch:[2, 200^{sgm.}, 100^{sgm.}, 50^{sgm.}, 2], $\lambda=0$, $\eta(\text{ADAM})=0.01$



$R(x, y, \sigma = 0.1/0.3)$, Arch:[2, 200^{sgm.}, 100^{sgm.}, 50^{sgm.}, 2], $\lambda_{L1, L2} = 10^{-4}$, $\eta(\text{ADAM})=0.01$

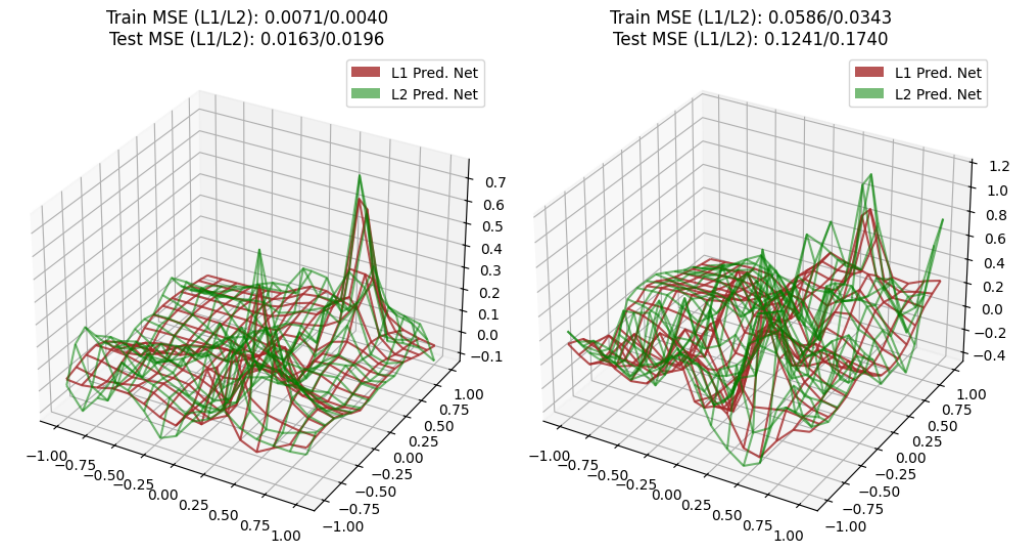


Figure 6: Applying ANN to a two-dimensional Runge function $R(x, y, \sigma)$, with noise levels $\sigma \in (0.1, 0.3)$. Each title states the noise, node number and activation for each hidden layer, and specifies the hyperparameters. **Top:** Using the same architecture as in Case 1, fails to adequately resolve the two signal peaks. **Mid:** Expanding the network with a third hidden layer, using sigmoid activation and a funnel-shaped node layout yields improved signal resolution, but the model becomes more sensible to background fluctuations leading to a degradation of signal efficiency and prediction variance when stronger noise is applied. **Bot:** Regularization is applied to mitigate overfitting. Stronger regularization $\lambda > 10^{-4}$ is seen to smoothen the background fluctuations but can damage the signal reconstruction. Ridge ($L2$) is generally more restrictive, while Lasso ($L1$) achieves a better tradeoff while reducing severe fluctuations of highly stochastic data sample.

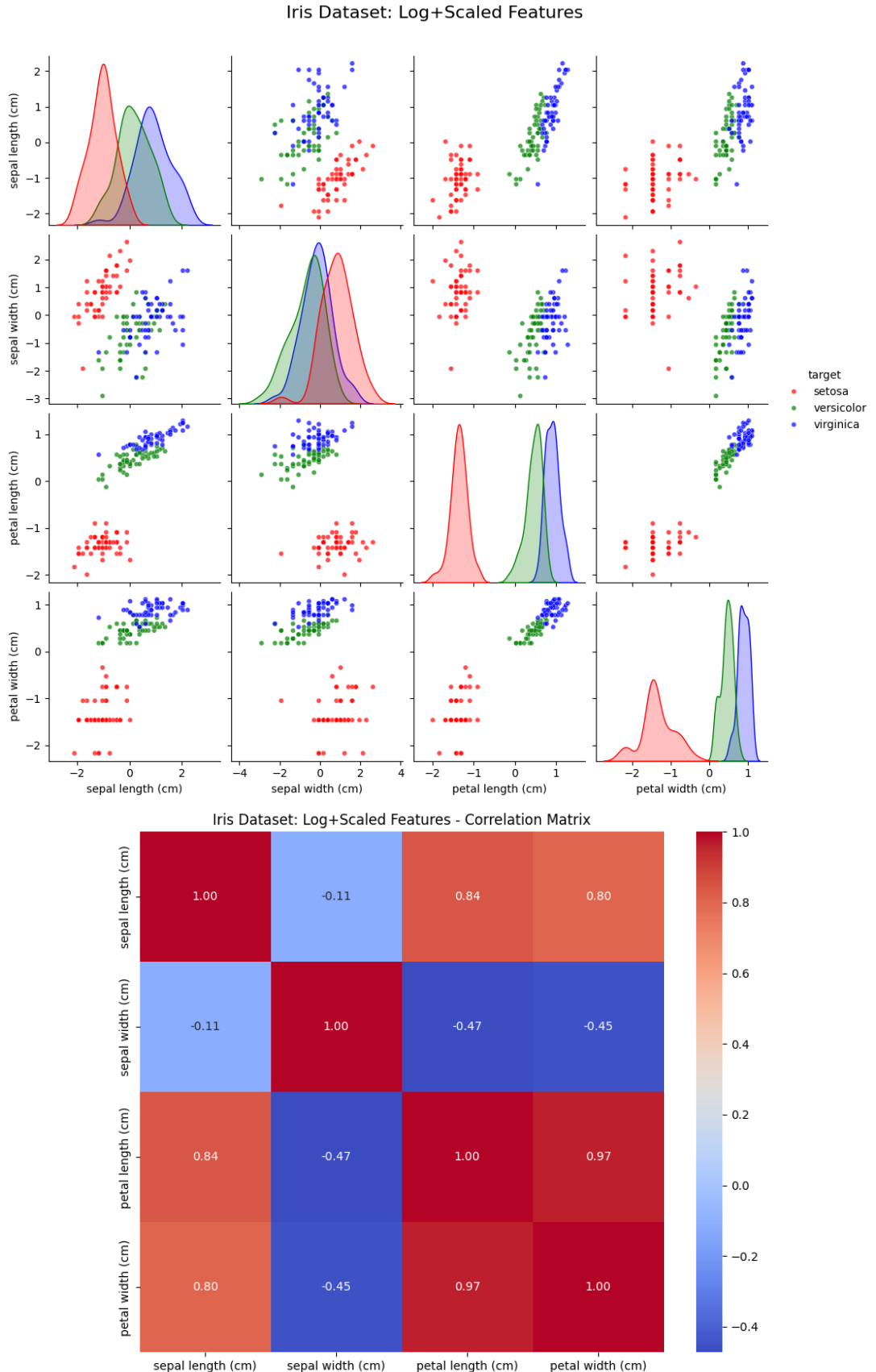


Figure 7: Iris data to be used for multiclass classification. This is a small dataset with 150 entries and 4 features: width/length of the flower sepal and petal. **Top:** The data processed as described in section II E, with logarithmic transform before applying standard scaling. Since all measurements are recorded in the same unit (cm.), with small magnitudes, this transformation failed to separate the distribution overlap (see diagonal plots). *Setosa* (red) is distinctly separated from the other two classes, while *Versicolor* (green) and *Virginica* (blue) have a large overlap based on sepal measures, with less critical overlap in petal features. Note that *Setosa* data has larger variance compared to *Virginica* with fewer outliers. **Bottom:** As expected, width and length are highly correlated features. Petal dimensions are particularly dependent on other features. Although this feature redundancy is disadvantageous, without existing substitutes, removing features would risk loosing discriminative information.

For classification optimization, we keep the previous successful GD and regularization parameters and define a new network architecture:

Case 2:

$$n_l \in \{4, 8, 3\}, \sigma^l \in \{\text{LReLU}, \text{LReLU}, \text{Softmax}^*\},$$

$$\text{ADAM}(\eta = 0.05), \text{Batch mode}, \lambda = 10^{-4}(L1)$$

*Batched Normalization

Based on arguments made in section II C we use Leaky ReLU for the hidden layers, and for the final layer, Softmax with batch normalization. Although the dimensionality of the problem ($n_0 = 4, n_L = 3$) could suggest the need for a deeper network, as was the case for regression in higher dimensions, an accuracy of 97% was achieved with a single hidden layer and relatively few nodes. Such accuracy is considered appropriate for simple ANNs without f.ex. convolutional stages. Attempts to further improve accuracy by using deeper networks with more nodes in the first layer showed no significant changes to the performance. Previously mentioned issues with the features are considered the main hindrance preventing further performance improvement. While sparse data for training can be handled using resampling techniques like Bootstrapping[2], with ineffective feature selections optimization is unlikely to reach accuracies in the range of 99 – 100%.

Furthermore, given the small datasets, it is reasonable to suggest regression as an alternative. Indeed, for binary classification predicting well-separated *Setosa* would be achievable, but with multiple classes containing overlaps and outliers, it is clear that traditional regression with linear or logistical separation would lead to many misclassifications.

Detailed results and class-wise performance is shown in Fig.5. The confusion matrix (top plot) shows that most predictions are correct dominant diagonal, with some cases of class 1 (*Versicolor*) mislabeled as 2 (*Virginica*) due to their overlapping feature distributions. The ROC curves (mid) confirm this, as class 0 (*Setosa*) with most separated distribution achieves the highest class discrimination, $AUC \approx 1$, with the other classes exhibiting slightly worse statistic. The gain curve (bot) indicate that > 0.9 of all true positives are recovered within 0.2 – 0.3 of the data. The steepest gain corresponds to *Virginica*, the class with lowest variance and few outliers.

D. Cancer Data: Binary classification

The last case is binary classification, $n_L = 2$, using the Wisconsin Breast Cancer data. This dataset is larger, with $M = 569$ entries, but unlike the Iris data, the entries are not evenly distributed with 212 *malignant* classifications and 357 *benign*. The target data is classified

based on 30 features describing the mean, worst and error measures of tumor properties: *radius*, *area*, *perimeter*, *texture*, *compactness*, *smoothness*, *concavity*, *concave points*, *symmetry* and *fractal dimension*. Many of these features are expected to be correlated, for instance, *radius* and *area*, while others, like *fractal dimension*, are not indicative of whether a case is benign or malignant. Fig.8 shows 4 selected features chosen for their low overlap and minimal correlation. The distributions (top) are the result of logarithmic transformation and consecutive scaling, except *worst concave points* whose log-transform distorted its distribution. Here, features represent different types of attributes and scaling is crucial. The correlation matrix (bottom plot) shows low dependencies, except for *concave points* which remains correlated with both *area* and *compactness*. Despite this, *concave points* has one of the highest discriminative values, and is therefore preserved.

We reuse Case 2 configuration as base, keeping the same activations on the grounds of arguments made in section II C and eq.14. Starting with a single hidden layer of 10 nodes, see top panel of Fig.9, accuracy of 95.1% or more specifically, $TF = 0.4, FP = 0.06$, where the latter refers to malignant cases classified as benign. The ROC curves exhibit high AUC for both classes. Despite the data imbalance, the data tends to belong to general regions in feature space. The Gain curves indicate a lasting drawback: ~ 0.5 and ~ 0.7 of malignant and benign data, respectively, must be sampled to recover all true positives. This is likely indicating malignant outliers deep inside the benign feature space as seen in Fig.8. Taking the preemptive log-transformation can to certain extent prevent this, though its highly specific on feature distributions and magnitudes. Considering *malignant* as rare yet valuable cases, we are particularly interested in increasing the gain rate of the model.

One reason could be insufficient model complexity. Performance results of a deeper network with $n_l \in \{30, 40, 20, 6, 2\}$, and $\lambda(L1) = 5 \times 10^{-3}$ are shown in the middle panel. The overall accuracy did not change, but we notice increased FP and lower FN , an unwelcome development, though certain variations to these numbers are expected. The ROC and gain rise improved, with all malignant TPs recovered around 0.4. Further extending the network with 4 hidden layers and larger number of nodes in n_2 did not give significant advances in neither the gain rate nor the FP statistic.

Finally, we make sure to use all available features, without log-transform, but retaining the standardization. With the same 3 hidden layers, it is possible to achieve 96.5% accuracy with $FP = 0.04$ and $FN = 0.03$. However, from 9 (bottom panel), the ROC and gain performance degraded. This confirms that while adding more features intuitively increased the accuracy statistics, the ROC and gain curves require a more qualitative approach, with individual handling of outliers, overlaps and correlations.

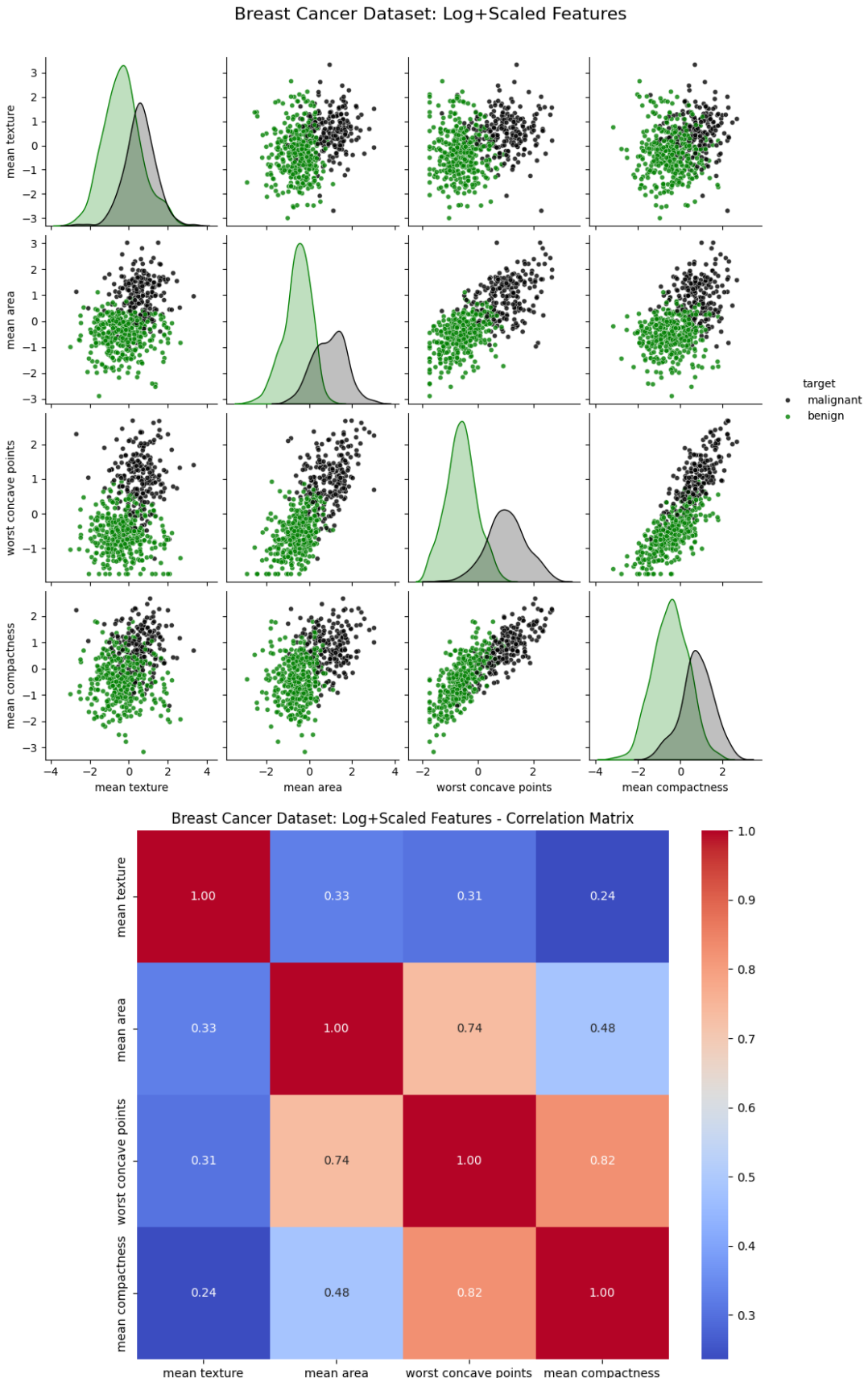


Figure 8: Wisconsin Breast Cancer Data to be used for binary classification. The dataset contains 569 entries and 30 features, many of which are strongly correlated, with some offering low discriminative power. **Top:** Displays the distributions of 4 selected features preprocessed according to section II E (except *worst concave points*, which was not log-transformed). Standardization of features is essential due to differing measurement scales in use. The chosen features provide strong discrimination with minimal overlap, as seen in the diagonal plots. **Bot:** The correlation matrix shows that *concave points* correlated more than wanted with both *compactness* and *area*, yet it is retained due to its classification value.

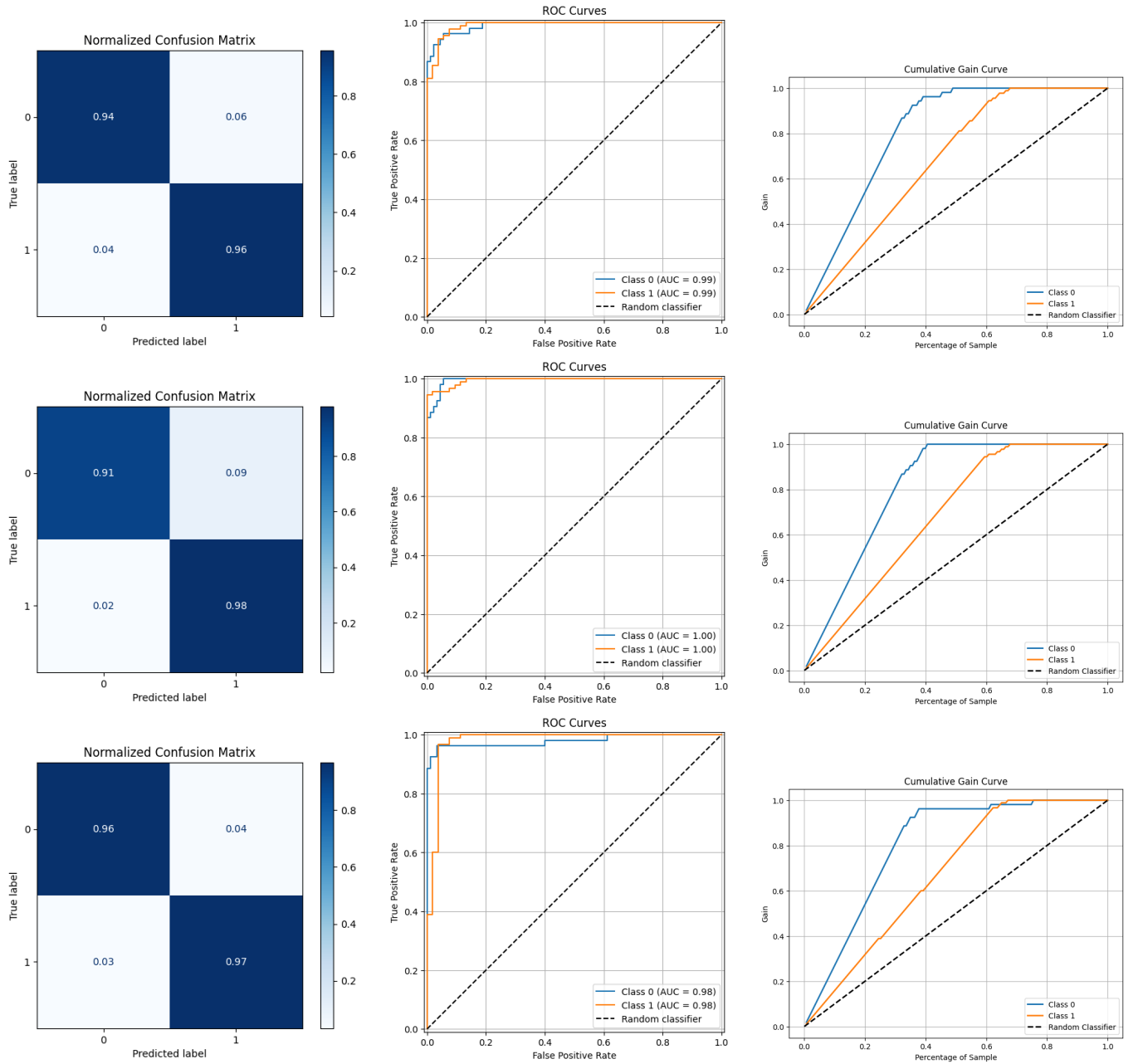


Figure 9: Performance of ANN binary classification on the Wisconsin Breast Cancer dataset. The dataset contains $M = 569$ entries with $n_0 = 30$ features and two output classes: *benign*, *malignant*. **Top:** Single hidden layer with $n_l = \{30, 10, 2\}$ achieves 95.1% accuracy with $FP = 0.06$, $FN = 0.04$. Despite fewer malignant samples, both ROC curves indicate good separation in feature space. The gain curve is less steep due to outliers. **Middle:** Deeper network with $n_l = \{30, 40, 20, 6, 2\}$ and $\lambda(L1) = 5 \times 10^{-3}$ shows no overall accuracy improvement. However, the performance of the ROC and Gain curve was improved as evidenced by the AUC and the percentage of samples at which all TP are recovered. **Bottom:** Using all 30 features without log transform but with standardization increases accuracy to 96.5%, yet the ROC and Gain curves degraded. This confirms that these statistics rely more on qualitative aspects of features, like overlaps, outliers and correlations.

IV. CONCLUSION

Our study demonstrates that neural networks with customizable Feed Forward architecture provide a universally applicable and sufficient framework for a diverse set of regression and classification tasks. By abstaining from convolutional or recurrent stages we confirm that the core structure is capable of predicting non-trivial functions and high-dimensional data to a satisfactory precision. The network model outperformed traditional polynomial regression for the one-dimensional Runge function, while displaying stable performance and ability to trace the true pattern even in harsher signal-to-noise ratios.

In case of higher dimensional inputs the network complexity can be scaled by using more hidden layers and greater number nodes. This alone does not guarantee improvement, as was seen with the two classification problems. A pressing concern with larger networks is overfitting, which we showed becomes increasingly difficult to solve relying on simple optimization measures such as regularization. Additional sophisticated safeguards, often inherent in specialized architectures like convolutional and recurrent networks become necessary to be able to process large feature sets. We also noted the prospects of redefining data representations like coordinate systems, as an preemptive step before training.

The flexibility of NNs comes with a less intuitive design process compared to traditional methods. While a polynomial regression's complexity is often encapsulated in a single parameter like degree P , a network's performance hinges many attributes, including layer dimensions, activation function, optimization parameters and trigger parameter initialization (which in this study was done at random). Tuning these typically requires ei-

ther substantial pre-knowledge of the data's properties or a resource-intensive process of trial and error. With the Runge function, we knew from previous analysis about the challenges with fitting the shape, hence we used the sigmoid. The necessity for intuition, is sometimes necessary as when applied to solving differential equations, one must know physical constraints like initial and boundary conditions.

For classification studies a large challenge comes embedded in the assisted learning aspect with preparing the data itself as large volumes of labeled data shifts the primary cost from the computational training process itself to the often expensive task of data acquisition and annotation.

This challenge is compounded by the central role of data quality and preparation. We found that performance is tightly constrained by inadequate data processing. This is particularly critical for classification, as demonstrated with the Wisconsin and Iris datasets, where performance relies more on the qualitative, discriminative value of features than their quantity. The presence of distributional overlaps and outliers directly impacts discrimination confidence and the efficient recovery of true positives. While future studies incorporating convolutional or recurrent layers may automate some feature extraction, the fundamental observations about data quality will remain essential for any practical application.

Furthermore, the distinction between data types—continuous outputs for regression and discrete for classification—remains a fundamental consideration. The assumption that the same architecture and activations are universally optimal is challenged when dealing with data streams that blur this line, opening an important discussion for pre-training data handling.

-
- [1] M. Hjorth-Jensen, *Computational Physics Lecture Notes 2015* (Department of Physics, University of Oslo, Norway, 2015), week: 37, 41, 42, 43, URL https://compphysics.github.io/MachineLearning/doc/LectureNotes/_build/html/intro.html.
 - [2] A. Umansky, FYS-STK3155 - Project 1 (2025), unpublished project report, University of Oslo, URL <https://github.com/4Lexium/Data-Analysis-and-Machine-Learning/tree/main/project1>.
 - [3] A. Peirce, *Runge phenomenon and piecewise polynomial interpolation (lecture 3)* (2017), accessed October 5, 2025, URL https://personal.math.ubc.ca/~peirce/M406_Lecture_3_Runge_Phenomenon_Piecewise_Polynomial_Interpolation.pdf.
 - [4] scikit-learn Developers, *sklearn.datasets.load_breast_cancer: Breast cancer wisconsin (diagnostic) dataset*, https://scikit-learn.org/stable/modules/generated/sklearn.datasets.load_breast_cancer.html (2025), accessed 2025.
 - [5] scikit-learn Developers, *sklearn.datasets.load_iris: Iris flower dataset*, https://scikit-learn.org/stable/modules/generated/sklearn.datasets.load_iris.html (2025), accessed 2025.
 - [6] I. Goodfellow, Y. Bengio, and A. Courville, in *Deep Learning* (MIT Press, 2016), accessed October 5, 2025, URL <https://www.deeplearningbook.org/contents/optimization.html>.
 - [7] T. Kurbiel, *Derivative of the softmax function and the categorical cross-entropy loss* (2021), medium – TDS Archive; accessed 2025, URL <https://medium.com/data-science/derivative-of-the-softmax-function-and-the-categorical-cross-entropy-loss-3a2a2a2a2a2a>.
 - [8] T. Hastie, R. Tibshirani, and J. Friedman, *The Elements of Statistical Learning: Data Mining, Inference, and Prediction, Second Edition. Springer Series in Statistics* (Springer, New York, 2009), URL <https://link.springer.com/book/10.1007%2F978-0-387-84858-7>.
 - [9] F. Pedregosa, G. Varoquaux, A. Gramfort, V. Michel, B. Thirion, O. Grisel, M. Blondel, P. Prettenhofer, R. Weiss, V. Dubourg, et al., *Scikit-learn: Machine Learning in Python* (2011), URL <https://scikit-learn.org/stable/>.
 - [10] C. R. Harris, K. J. Millman, S. J. van der Walt, R. Gommers, M. E. Virtanen, D. Cournapeau, E. W. Larson, T. Allaire, J. Berg, N. J. Smith, J. J. scikit-learn Developers, *scikit-learn: Simple and efficient statistical modeling in Python*, https://scikit-learn.org/stable/modules/generated/sklearn.datasets.load_iris.html (2025), accessed 2025.

- mers, P. Virtanen, D. Cournapeau, E. Wieser, J. Taylor, S. Berg, N. J. Smith, et al., *NumPy: Array programming with Python* (2020), URL <https://numpy.org/>.
- [11] D. Maclaurin, D. Duvenaud, and R. Adams, *Autograd: Effortless Gradients in Python* (2015), URL <https://github.com/HIPS/autograd>.
- [12] J. D. Hunter, *Matplotlib: A 2D Graphics Environment* (2007), URL <https://matplotlib.org/>.
- [13] M. Waskom, *Seaborn: Statistical Data Visualization* (2021), URL <https://seaborn.pydata.org/>.
- [14] M. Abadi, A. Agarwal, P. Barham, E. Brevdo, Z. Chen, C. Citro, G. S. Corrado, A. Davis, J. Dean, M. Devin, et al., *TensorFlow: Large-Scale Machine Learning* on *Heterogeneous Systems* (2016), URL <https://www.tensorflow.org/>.
- [15] T. O’Malley et al., *Keras Tuner* (2019), URL https://keras.io/keras_tuner/.
- [16] I. Goodfellow, Y. Bengio, and A. Courville, *Deep Learning* (MIT Press, 2016), <http://www.deeplearningbook.org>.
- [17] A. Mandilara, B. Dellen, U. Jaekel, T. Valtinos, and D. Syvridis, *Quantum Machine Intelligence* **6**, 17 (2024), URL <https://link.springer.com/article/10.1007/s42484-024-00146-3>.